# Onset of Hydrogen Bonded Collective Network of Water in 1,4-Dioxane

Trung Quan Luong,[†] Pramod Kumar Verma,[‡] Rajib Kumar Mitra,[‡] and Martina Havenith*,[†]

[†]Department of Physical Chemistry II, Ruhr-University Bochum, 44780 Bochum, Germany

[‡]Unit for Nano-Science and Technology, Department of Chemical, Biological and Macromolecular Sciences, S.N. Bose National Centre for Basic Sciences, Block JD, Sector III, Salt Lake, Kolkata 700098, India

Ⓢ *Supporting Information*

ABSTRACT: We have studied the evolution of water hydrogen bonded network dynamics in mixtures of 1,4-dioxane (Dx) as the mole fraction of water (X_w) increases from 0.005 to 0.54. The inter- and intramolecular vibrations of water have been observed using terahertz time domain spectroscopy (THz-TDS) in the frequency range 0.4–1.4 THz (13–47 cm^{-1}) and Fourier transform infrared (FTIR) spectroscopy in the far-infrared (30–650 cm^{-1}) and mid-infrared (3000–3700 cm^{-1}) regions. These results have been correlated with the reactivity of water in these mixtures as determined by kinetic studies of the solvolysis reaction of benzoyl chloride (BzCl). Our studies show an onset of intermolecular hydrogen bonded water network dynamics beyond $X_w \geq 0.1$. At the same concentration, we observe a rapid increase of the rate constant of solvolysis of BzCl in water–Dx mixtures. Our results establish a correlation between the onset of collective hydrogen bonded network with the solvation dynamics and the activity of clustered water.
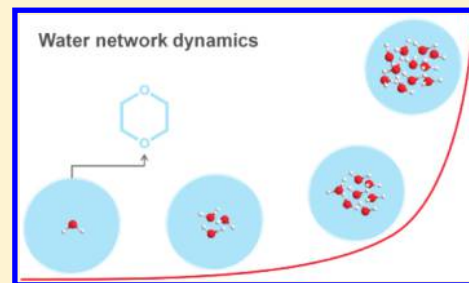
■ INTRODUCTION

Water plays an important role in many chemical and biological processes.[1−3] While the structure of most of the liquids is dominated by repulsive forces, the additional attractive hydrogen bonding interactions in water lead to its unique properties.[4] Water in hydrophobic environment forming clathrate clusters of 2−10 water molecules can give rise to properties different from those of bulk water. In general, entropy and van der Waals forces are thought to play a crucial role.[5−9] The interaction of polar water molecules with a hydrophobic/hydrophilic surface influences the dynamics of water molecules (or small water clusters) in the vicinity of the surface. Although hydrogen bond dynamics in bulk water and near hydrophobic molecules have been intensively studied with many techniques,[10−12] very little is known about the co-operativity and microheterogeneity in mixed solvents on a molecular level.

In this article, we report the study of mixtures of water and 1,4-dioxane (Dx) using terahertz time domain spectroscopy (THz-TDS) and Fourier transform infrared (FTIR) spectroscopy. In spite of being a nonionic and nonpolar solvent, Dx can solubilize water from highly diluted to highly concentrated mixtures and also exposes a substantial number of noninteracting sites (the hydrophobic segments) to water molecules. Dx molecules do not self-associate; however, they are capable of forming hydrogen bonds with water. Water−Dx bonds that replace the water−water hydrogen bonds are weaker than the corresponding water−water hydrogen bonds.[13] In mixtures with highly diluted concentrations of water, the three-dimensional water−water hydrogen bond network is disrupted. Such situation resembles that of isolated

water molecules with fewer interactions to other water molecules. This provides a unique opportunity to study properties of nearly isolated water molecules (i.e., those which are not hydrogen bonded with other water molecules).[14−17]

A considerable number of studies in water−Dx mixed systems have been reported earlier, including thermodynamic parameter of mixing,[13,18,19] IR spectroscopy,[20−22] NMR relaxation,[23,24] time domain reflectometry,[25] time-resolved fluorescence spectroscopy,[26−28] dielectric relaxation,[29−32] etc. Using dielectric relaxation in the frequency range of 0.1−10 GHz, Mashimo et al.[32] reported the formation of cyclic water structures at high water concentrations (mole fraction of water $X_w > 0.83$). However, in recent studies using a wider range of frequency, Schrödle et al.[30,31] concluded that the cooperative hydrogen bonded network relaxation can be found even at very low water concentrations. Near infrared (NIR) studies by Choppin et al.[21] identified three different species of water molecules in Dx and proposed that these form 0, 1, and 2 hydrogen bonds. A very recent femtosecond-resolved (fs-resolved) fluorescence spectroscopic study[26] reported very fast dynamics of water molecules in small water clusters at low X_w, which slows down for higher water concentrations ($X_w \geq 0.2$). In the same study, a gradual increase of water cluster size with increasing X_w was detected using the dynamic light scattering (DLS) technique.

IR-vibrational spectroscopy is a well-known technique to investigate the structure and hydrogen bonding of water molecules.[33–35] Characteristic symmetric and asymmetric O−H stretching bands of water molecules are found in the frequency range 3000−3700 cm^{-1}.[36,37] Further bands of water are found around 2100 cm^{-1} (coupled bending and librational motions), 1650 cm^{-1} (bending), 600 cm^{-1} (libration), and 200 cm^{-1} (intermolecular hydrogen bond stretching vibrations).[38–40] The intermolecular vibrational modes at frequencies above 300 cm^{-1} are attributed to librational (i.e., hindered rotational) motions.[41,42] Our recent ab initio simulation study[43] identifies the collective nature and delocalized character of these low frequency modes, which involve correlated particle motions extending over several hydration shells: while the prominent peak at 200 cm^{-1} is dominated by the first shell dynamics, a concerted particle motion involving the second hydration shell contributes to the absorption around 80−90 cm^{-1}.

The present study focuses on three different aspects of the evolution from weakly to strongly bonded water clusters in Dx, namely, (a) how the structure changes with X_w, (b) how this change in the structure is related to the water dynamics, and (c) how these changes in dynamics are correlated with the activity of water. Initially, we start with a low concentration of water ($X_w = 0.005$) in order to minimize any intermolecular water interactions. The mole fraction of water is then gradually increased up to 0.54. The formation of the water network is studied in the far-infrared (FIR) and mid-infrared (MIR) regions using FTIR spectroscopy. The slow and fast water dynamics are investigated by using dielectric relaxation data obtained from THz-TDS. Activity of these water molecules is described by measuring the kinetics of solvolysis of benzoyl chloride (BzCl). Our studies show a systematic change in the dynamics and hydrogen bonding with variation of X_w. These changes can be directly correlated with a change in the activity.

■ EXPERIMENTAL METHODS

Dx (99% or higher purity) and BzCl were purchased from Sigma Aldrich and were used without further purification. Water−Dx mixtures were prepared by dissolving water in Dx. Water concentration is expressed in terms of mole fractions of water (X_w). For FTIR and THz-TDS measurements, the liquid samples were placed in a liquid sample cell (model A145, Bruker Optics) with a Teflon spacer placed between two parallel windows. Diamond windows were used for FTIR measurements in the FIR region, while z-cut quartz windows were used for MIR-FTIR and THz-TDS measurements. Spacers with suitable thicknesses were chosen depending on the absorbance of the samples, which increases with increasing water concentration. The precise cell thicknesses were determined by the measurement of etalon fringes using FTIR spectroscopy. Kinetics measurements were carried out in a quartz cuvette of 1 cm path length.

FTIR Measurements. FTIR spectra were recorded using a VERTEX 80v FTIR Spectrometer (Bruker Optics) at 20 ± 0.2 °C under nitrogen gas flow in the sample compartment. The data were collected and processed using OPUS software. For spectra acquisition in the MIR region (3000−3700 cm^{-1}), we used a built-in MIR source of the spectrometer and an MCT (Mercury−Cadmium−Telluride) detector. A cell thickness of 52.6 μm was used for X_w ranging from 0 to 0.19 and a cell thickness of 28.5 μm for X_w ranging from 0.26 to 0.54. In the FIR region (30 to 650 cm^{-1}), a mercury-lamp served as an FIR source, a liquid-helium-cooled
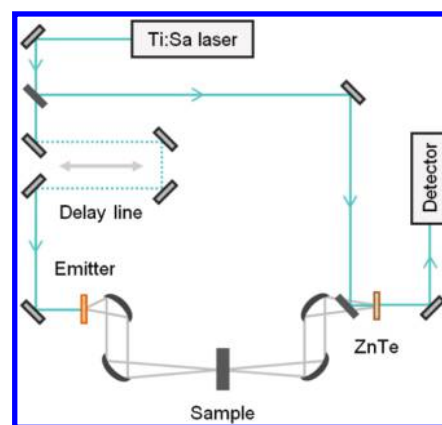

Figure 1. Schematic diagram of the THz-TDS setup. The femtosecond laser pulses emitted from the Ti:Sa laser are split into two parts (pump pulse and probe pulse). The pump pulse propagates via a mechanical delay line to adjust the time delay between the probe and the pump pulse and is used to generate THz pulses via a THz emitter. The probe pulse is used for coherent electro-optical detection of the THz signal.

silicon bolometer was used as a detector. The cell thickness was fixed to 52.6 μm for all water−Dx mixtures and 12.0 μm for pure water.

THz-TDS Measurements. The THz responses of the samples were obtained using a THz-TD spectrometer (Figure 1). The continuous-wave laser (Verdi, Coherent) emits laser light at 532 nm and serves as a pump source for the Ti:Sa laser (KMLabs Inc.), which produces mode-locked laser pulses of 20 fs (fs) duration with an 80 MHz repetition rate and 500 mW optical output power. The laser beam is then split into two parts (pump pulse and probe pulse). The first part (pump pulse) propagates via a mechanical delay line which allows to adjust to a controlled time delay (Δt) between pump and probe pulse. The pump pulse is focused on the THz emitter (Tera-SED, Gigaoptics) for generation of THz pulses. A system of four parabolic mirrors focuses the THz beam on the sample and afterward on the nonlinear (110)ZnTe crystal. The probe pulse is also focused onto the ZnTe crystal. The electric field of the THz pulse changes the optical properties of the nonlinear ZnTe crystal due to Pockel's effect. This results in a rotation of the linear polarized fs probe pulses. The rotation of linear polarization of the fs probe pulse is proportional to the electric field of the THz beam (E_{THz}). This coherent electro-optical detection scheme is very sensitive. By varying the time delay Δt, we can measure E_{THz} as a function of time. To avoid water vapor absorption, the THz setup is enclosed in a box, which is purged with dry air. All THz-TDS measurements were carried out under thermal equilibration (humidity at 5.0 ± 0.1% and temperature at 20 ± 0.2 °C). Because of high water absorption in the THz frequency range, we varied the cell thicknesses depending on water concentration (cell thicknesses of 1.54, 1.03, and 0.21 mm for X_w ranging from 0 to 0.023, 0.034 to 0.19, and 0.26 to 0.54, respectively) to guarantee the penetration of the laser pulse. Using the measured time-dependent electrical field $E_{THz}(t)$ as an input, a fast Fourier transformation was applied to obtain the frequency-dependent power and phase of the transmitted pulse. Subsequently, the frequency-dependent absorption coefficient $\alpha(\nu)$ (power attenuation), index of refraction $n(\nu)$ (delay of the THz pulse) as well as the complex dielectric constant $\hat{\varepsilon}(\nu) = \varepsilon'(\nu) - i\varepsilon''(\nu)$ were deduced.[44]

Kinetics of BzCl Solvolysis. The kinetics of the BzCl solvolysis reaction was determined by measuring the temporal change

14463

dx.doi.org/10.1021/jp204927r |*J. Phys. Chem. A* 2011, 115, 14462–14469

in the absorbance of BzCl monitored at 288 nm using a Shimadzu UV-2450 spectrophotometer. The rate of the reaction was calculated using a first order exponential fit of the absorbance data. The initial BzCl concentration was kept constant at $\sim$10 μM.
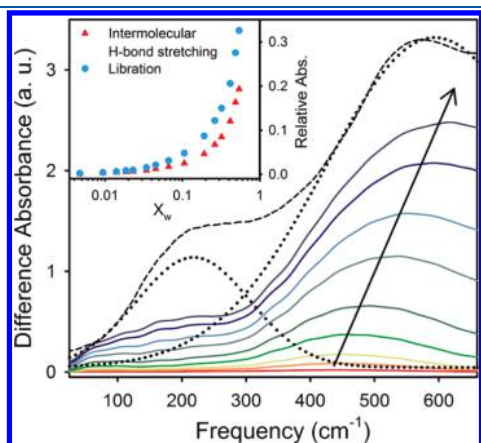

Figure 2. Difference absorption spectra of water—Dx mixtures in the FIR region with X_w = 0.005, 0.023, 0.045, 0.11, 0.19, 0.32, 0.42, 0.49, and 0.54 (from bottom to top). The spectrum of water (broken line) in an adjusted scale is shown for comparison. The dotted lines are the deconvoluted spectra of the water absorption spectrum. The arrow marks the progressive blue shift of the libration band with increasing water concentration. The inset shows the relative absorption coefficient (compared to water) for the two vibrational modes: intermolecular hydrogen bond stretching (arsing $\sim$200 cm^{-1} in water) and libration mode (arising $\sim$600 cm^{-1} in water).

■ RESULTS AND DISCUSSION

Structure. In Figures 2 and 3, we present the FTIR spectra of water—Dx mixtures in the FIR (30—650 cm^{-1}) and MIR (3000—3700 cm^{-1}) regions, respectively. In order to extract structural information, we have calculated the difference between the absorbance spectra of the mixtures and the absorption spectrum of pure Dx. The absorption of Dx in the FIR and MIR regions is found to be almost negligible, except for two strong Dx absorption bands in the FIR region centered at 280 and 610 cm^{-1} (Figures S1 and S2 in the Supporting Information). In the resulting difference absorbance spectra, we smoothed the data between these two high absorption regions to ensure that they follow a continuous trend of the spectra before and after these regions. The obtained difference absorbance spectra are attributed solely to the partial contribution of water in water—Dx mixtures.

FIR. The spectrum of pure water in the FIR region shows two characteristic peaks at $\sim$200 and $\sim$600 cm^{-1} (Figure 2). We deconvoluted the observed water spectrum into two separate bands centered at 200 and 600 cm^{-1}. As discussed earlier, the former one is assigned to the intermolecular hydrogen bond stretching vibrations, while the latter one to the libration.[38,39,45,46] For the mixed systems at low water concentrations (X_w < 0.1), a maximum absorption is found around 450 cm^{-1}, while almost no peak can be seen at 200 cm^{-1}. With an increase in X_w, the libration peak shows a progressive blue shift, and for X_w = 0.54, the spectrum resembles that of pure water. In the inset of Figure 2, we plot the relative absorbance of water—Dx mixtures (measured at the maximum) compared to that of bulk water (measured at the maximum) in the region of the intermolecular stretching
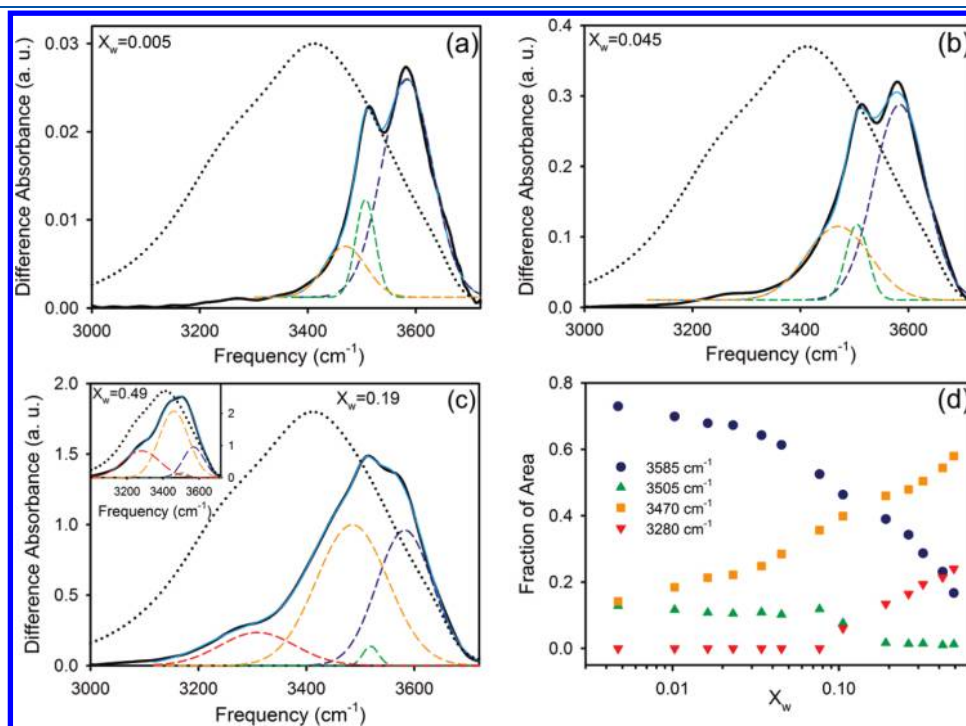

Figure 3. MIR difference absorbance spectrum (black solid line) in the O—H stretching frequency range of water—DX mixtures with X_w of 0.005 (a), 0.045 (b), 0.19 (c), and 0.49 (c, inset). The spectra in panels a and b are deconvoluted into three different spectra centered at 3585, 3505, and 3470 cm^{-1} shown by blue, green, and orange broken lines, respectively. The cyan lines represent the overall fit of the total spectra. The dotted black line is the curve for pure water absorption drawn in an adjusted scale for comparison. For X_w = 0.19 and 0.49, the spectra are deconvoluted into four different spectra with one more spectrum centered at 3280 cm^{-1} (red broken lines). (d) Fraction of area under the curve for each deconvoluted spectrum centered at 3585, 3505, 3470, and 3280 cm^{-1}.

and libration bands. The libration mode always has a higher relative absorbance compared to the intermolecular hydrogen bond stretching vibration.

The obtained FIR spectra can be discussed in the light of the previously studied water−acetone (AC) or water−acetonitrile (AN) spectra in this region.[47] These previous studies reveal a progressive blue shift of librational band with increasing water content in the mixtures. The most pronounced effect for both the mixed systems was observed in the water diluted region. At 0.1 volume fraction of water, the maximum peak position was shifted from ∼670 cm^{-1} to 500 cm^{-1}.[47] The shape and position of the spectrum depends on the hydrogen bonding character in the solutions.[48,49] In a binary aqueous mixture, the number of water molecules that act as hydrogen bond donors is approximately independent of the concentration.[50] However, the number of water molecules that serve as hydrogen bond acceptors decreases rapidly when decreasing the water concentration ($X_w \leq 0.7$). Accordingly, more and more water molecules become hydrogen bond donors to cosolvent molecules in the water diluted region.[47] For $X_w < 0.2$, only a small fraction of water molecules are hydrogen bonded to more than two water molecules. Instead, water molecules bind preferentially with cosolvents, thereby forming less strong hydrogen bonds.

Our recent simulation study[43] revealed that the low frequency modes correspond to collective particle motions involving more than a single water layer (i.e., we found a correlation of the particle motion over more than 7 Å). Within the investigated concentration range, the relative absorbance (compared to that of pure water) of the libration mode (at 600 cm^{-1}) is found to be higher than the relative absorbance of the lower frequency mode at 200 cm^{-1} (Figure 2, inset). The mode at 200 cm^{-1} is assigned to the intermolecular collective vibration mode. This band is absent in the highly diluted (low X_w) region, which is explained by a breakdown of the hydrogen bonded network. With increasing water concentration ($X_w \geq 0.1$) a shoulder starts appearing in this frequency range, indicating the onset of the hydrogen bond network dynamics.

MIR. The MIR difference absorption spectra of the water−Dx mixtures in the frequency range of 3000−3700 cm^{-1} are shown in Figure 3. Figure 3a shows the difference spectrum for a mixture with $X_w = 0.005$ having two distinct peaks, which are blue-shifted from that of the pure water spectrum (shown in the dotted line, data taken from ref 38). These spectra are similar to the previously observed spectra for water−Dx[20] and water−AN[51] mixtures. In order to achieve a more quantitative understanding, we decompose the spectrum into three Gaussian sub-bands centered at 3585, 3505, and 3470 cm^{-1}. The deconvoluted spectrum of pure water shows two bands at 3470 and 3280 cm^{-1}, both having comparable intensity (Figure S3 in the Supporting Information). The two peaks are assigned to the intramolecular water OH stretch arising from weak and strong hydrogen bond conformations, respectively.

For the mixed systems, we assign the peak at 3470 cm^{-1} to an OH stretch of a water molecule, which is weakly hydrogen bonded to the nearby water molecule. A similar peak has also been found in the water−AN mixture (∼3450 cm^{-1}).[16] Nonbonded OH groups,[14,52] which are associated with the peaks between 3600 and 3700 cm^{-1}, could not be unambiguously assigned in the present study. The 3585 and 3505 cm^{-1} peaks are attributed to vibrational bands of water molecules that share hydrogen bonding with Dx, with weaker O−H stretch bonds compared to water−water hydrogen bond and red-shifted free OH bonds or
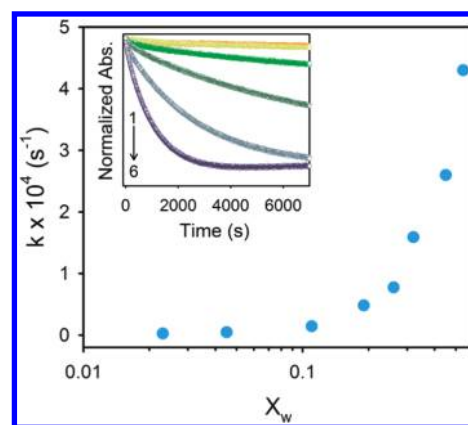

Figure 4. Rate constant (k) of solvolysis of BzCl in water−Dx mixtures at different mole fractions of water. The normalized absorbance decay as a function of time is shown in the inset at different X_w of 0.023 (1), 0.045 (2), 0.11 (3), 0.19 (4), 0.32 (5), and 0.54 (6).

dandling bonds.[52] The relatively high intensity of the 3585 cm^{-1} band suggests that such weakly bonded water molecules are highly abounded. As the concentration of water is increased to 0.045, the contribution of the 3470 cm^{-1} band grows with a consequent decrease in the contribution of the other two peaks.

At relatively high water concentrations ($X_w \geq 0.1$), the difference spectrum can only be fitted when assuming an additional band centered at 3280 cm^{-1} (Figure 3c). This band is assigned to the stretching band of the strong hydrogen bond network of water molecules, showing the onset of the formation of bulk water clusters. When further increasing the water concentration ($X_w = 0.49$), the difference spectrum resembles that of bulk water (Figure 3c, inset), and the major contribution stems from bands centered at 3470 and 3280 cm^{-1}. The spectra of the mixtures with $X_w \geq 0.1$ could be fitted with four components centered at 3585, 3505, 3470, and 3280 cm^{-1}, respectively. In Figure 3d, we plot the partial contribution of each (defined by the corresponding area) as a function of X_w. This plot correlates the relative population of different water species present in the mixtures. As observed from Figure 3d, the contribution of the 3585 cm^{-1} peak decreases first slowly and then rapidly, whereas those of the low frequency bands, especially the 3470 cm^{-1} band, increases gradually. Beyond $X_w = 0.1$, the first signature of a strong hydrogen bond appears in the form of a 3280 cm^{-1} band, and its contribution grows gradually with X_w. Thus, both MIR and FIR modes of vibration spectroscopy confirm a dramatic change in the solvent structure dynamics as a function of water concentration.

Activity. Figure 4 depicts the results of the kinetics of the BzCl solvolysis reaction in water−Dx mixtures at different X_w. As observed from the figure, the reaction is very slow in the low X_w region (rate constant, $k \approx 10^{-6}$ s^{-1}). The reaction rate increases significantly at $X_w \geq 0.1$. The observed rate constants at high X_w values are in good agreement with previously reported rate constants observed in similar systems.[53] However, these rate constants are even for high X_W values considerably slower than that in pure water (∼1 s^{-1}),[54−56] indicating poor reactivity of water in the mixture.

Dynamics. The dielectric spectra of water−Dx mixtures are measured using THz-TDS in the frequency range from 0.4 to 1.4 THz (13−47 cm^{-1}). The results are displayed in Figures 5 and 6. Frequency dependent absorption coefficient (α) and refractive index (n) of representative mixtures are plotted in Figure 5a.
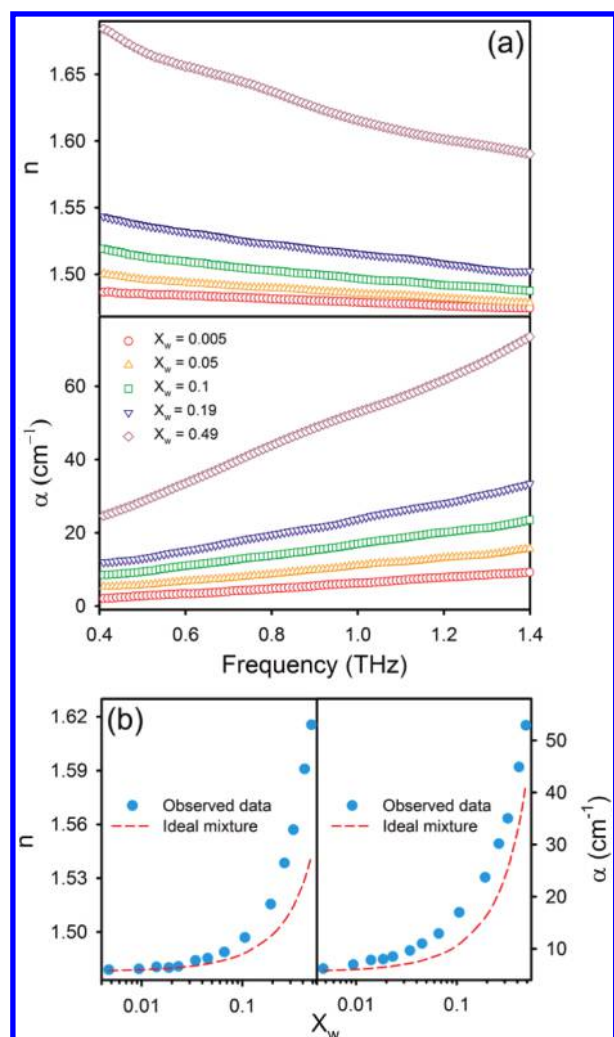
Figure 5. (a) Frequency dependence of refractive index (n) and absorption coefficient (α) of water−Dx mixtures at different mole fractions of water. (b) Observed and calculated (for ideal mixtures) n and α for water−Dx mixtures as a function of X_w at 1 THz frequency.

As observed from the figure, $n(\nu)$ decreases, while $\alpha(\nu)$ increases with frequency. Both $\alpha(\nu)$ and $n(\nu)$ increase with increasing water content.

Previous studies with water−AN mixtures yielded an increase in $n(\nu)$ and a decrease in $\alpha(\nu)$ with increasing water concentration,[60] whereas $\alpha(\nu)$ was found to increase with water content for water−AC and water−methanol mixtures.[47] The increase in $\alpha(\nu)$ with water content can easily be explained by taking into consideration that Dx has a very low $\alpha(\nu)$ compared to water in this frequency range.[31] For an ideal mixture, the absorption coefficient and the index of refraction can be calculated using the following relationship:[47]

$$A_{\mathrm{ideal}}(\nu) = \frac{\rho_{\mathrm{real}}}{\rho_{\mathrm{ideal}}} \sum_i V_i A_i(\nu) \qquad (1)$$

where, A_i is the absorption coefficient or index of refraction of the i-th species, V_i is the volume fraction of the i-th species in the solution, ρ_{real} is the density of the mixture, and ρ_{ideal} is the density of the ideal mixture assuming a two component model. The ratio $\rho_{\mathrm{real}}/\rho_{\mathrm{ideal}}$ is given here to account for small nonidealities in the volume upon mixing. We plot the observed α and n at different
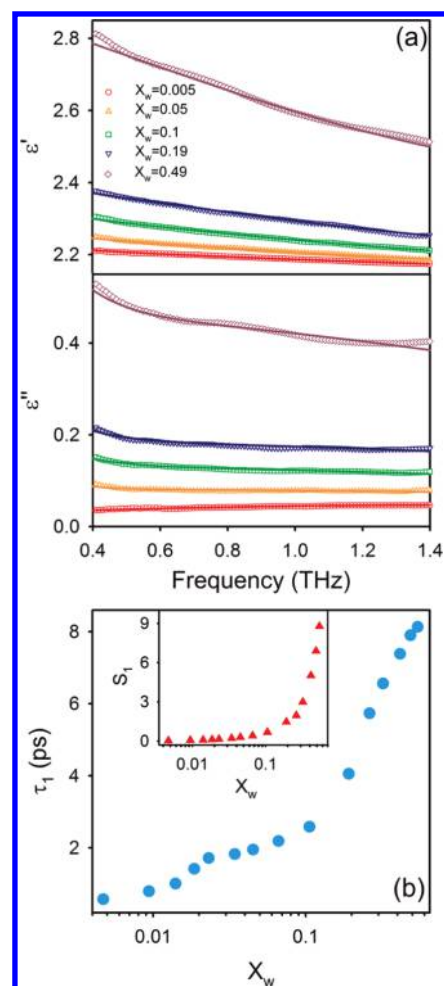

Figure 6. (a) Real (ε') and imaginary (ε'') part of the dielectric constant of water−Dx mixtures at different mole fractions of water. The solid lines represent the double Debye relaxation fitting. (b) Debye relaxation time constant (τ_1) for different water−Dx mixtures. The inset shows the related relaxation strength (S_1).

X_w values measured at 1 THz frequency in Figure 5b. The results as predicted, following eq 1 for ideal mixtures, are shown as a broken line in the same plot for comparison. As can be observed from the figure, the attempt to describe the mixtures as ideal mixtures fails, which indicates a significant change in the network by the addition of the solute. Similar results were also obtained for water−AN and water−AC mixtures.[47,60]

One of the most commonly used models to describe dielectric relaxation is the Debye model, which describes the dynamics in terms of collective, diffusive, and reorientational motions and has extensively been used for pure liquids and liquid mixtures.[29−31,47,61−63] According to the Debye model, the dielectric relaxation can be described as:

$$\hat{\varepsilon}(\omega) = \varepsilon_\infty + \sum_{j=1}^{n} \frac{\varepsilon_j - \varepsilon_{j+1}}{1 + i2\pi\nu\tau_j} \qquad (2)$$

where, τ is the relaxation time, ν is the frequency, $\varepsilon_1 = \varepsilon_s$ is the static dielectric constant, ε_j are dielectric constants for different relaxation processes, $\varepsilon_{n+1} = \varepsilon_\infty$ is the extrapolated value at high frequency, and n describes the number of relaxation processes that have been taken into account. The Debye model

Table 1. Double Debye Relaxation Fitting Parameters for Water–Dx Mixtures at Different Compositions

X_w	ε_∞	ε_s	ε_2	τ_1 (ps)	τ_2 (ps)	S_1	S_2
0.005	2.12	2.24	2.20	0.57	0.09	0.04	0.08
0.009	2.12	2.27	2.21	0.79	0.09	0.06	0.09
0.014	2.12	2.30	2.21	1.01	0.09	0.09	0.10
0.019	2.12	2.34	2.22	1.42	0.10	0.12	0.10
0.023	2.12	2.37	2.22	1.72	0.10	0.15	0.10
0.034	2.13	2.46	2.24	1.83	0.11	0.22	0.11
0.045	2.13	2.54	2.24	1.95	0.11	0.29	0.11
0.066	2.13	2.67	2.26	2.19	0.11	0.41	0.13
0.11	2.13	2.98	2.30	2.59	0.12	0.68	0.17
0.19	2.13	3.85	2.38	4.05	0.12	1.47	0.25
0.26	2.14	4.45	2.49	5.74	0.12	1.96	0.35
0.32	2.18	5.57	2.58	6.56	0.13	2.99	0.40
0.42	2.21	7.73	2.71	7.39	0.12	5.02	0.50
0.49	2.25	9.71	2.82	7.90	0.13	6.89	0.57
0.54	2.29	11.70	2.92	8.13	0.13	8.78	0.63

assuming $n = 1$ is the simplest case assuming that a single relaxation time provides an adequate description. The magnitude of induced polarization is given by the dispersion amplitude $S_j = \varepsilon_j - \varepsilon_{j+1}$. In many cases, the dielectric spectra can be adequately fitted to two independent relaxation processes

$$\hat{\varepsilon}(\nu) = \varepsilon_\infty + \frac{\varepsilon_s - \varepsilon_2}{1 + \mathrm{i}2\pi\nu\tau_1} + \frac{\varepsilon_2 - \varepsilon_\infty}{1 + \mathrm{i}2\pi\nu\tau_2} \qquad (3)$$

The results of a fit assuming two independent relaxation processes are given in Figure 6a, the fitted parameters for different X_w values are summarized in Table 1. In an earlier study, Garg et al.[29] reported a slow relaxation process (of the order of 20–50 ps) in the concentration range of $X_w = 0.2$ to 0.8 in water–Dx mixtures. Recently, Schrödle et al.[30,31] have made extensive studies on the dielectric relaxation of water–Dx mixtures at low water and low to moderate Dx concentration regions. Their results show a maximum in the time constants of the Debye relaxation processes (τ_1 and τ_2) as a function of X_w indicating cooperative relaxation behavior of water clusters. Our study provides complementary information on the onset of the cooperative relaxation process in the mixture and its manifestation in the structure and activity of water molecules.

Bulk water shows two characteristic relaxation processes,[44,61] one slow ($\tau_1 \approx 8$ ps) arising from the cooperative relaxation of the hydrogen bond network and another faster one ($\tau_2 \approx 0.1–0.4$ ps)[12,44,61] resulting possibly from the nonseparable contribution of the few free water molecules.[63,64] In the investigated frequency range, we are probing preferentially the slower processes. Therefore, we restrict our discussion to the change in τ_1 only. From previous studies,[31] it is known that neat Dx has no significant contribution at that time scale, so we probe here mainly the water dynamics. As a result of the present study, we find that at very low water concentration the relaxation data can be fitted to two relaxation processes with time constants of ∼0.6 and ∼0.1 ps (Table 1). The deduced τ_1 value obtained is considerably decreased compared to that of bulk water.

Figure 6b summarizes the results of the dielectric relaxation study. At low water concentration ($X_w < 0.1$), the τ_1 values are very small compared to that of bulk water and increase then from 0.6 to 2.5 ps. Since this mode of relaxation is mostly assigned to

the cooperative relaxation of the hydrogen bond network, the low τ_1 value indicates a lack of any cooperative network in the mixtures as has also been evidenced in the FTIR and kinetics study. At $X_w \geq 0.1$, τ_1 increases very rapidly, and at moderately high concentration of water ($X_w = 0.54$), the time scale approaches that of bulk water. This change shows a rapid onset of the collective network motions similar to what was observed in a previous study of solvated model peptides.[65]

The parameter S_1 ($S_1 = \varepsilon_s - \varepsilon_2$) describes the amplitude of the dielectric relaxation process with the slowest time constant (τ_1), as given in eq 3 in the article. τ_1 describes the cooperative relaxation time of the hydrogen bond network. When the concentration of water increases, more water molecules contribute to the hydrogen bond network. Thus, S_1 increases with the number of water molecules that participate in the hydrogen bond network. The plot showing S_1 as a function of the concentration of water (Figure 6b, inset) further supports the onset of a collective hydrogen bonded network for $X_w \geq 0.1$.

The results of the present THz-TDS study are in agreement with the results of a previous time-resolved fluorescence study for an identical system.[26] There, a fast solvent relaxation is found at low water concentration. At $X_w = 0.2$, an additional slow process develops, which is attributed to the translational diffusion of water molecules around the fluoroprobe. The suggested growth in the water cluster size with X_w has been reported before in an earlier dynamic light scattering (DLS) study of the same system.[26] In light of that, we can conclude that with the growth in the cluster size, the cooperative relaxation dynamics of water in the mixtures increases gradually and reaches a value identical to that of bulk water (Table 1).

■ CONCLUSIONS

Our present study combines three different experimental techniques with the primary objective to understand the evolution of water network structure in water–Dx mixtures. FTIR studies were aimed to unravel the evolution of the hydrogen bond formation by the shift of OH bond frequencies. Our results show a gradual increase of the collective hydrogen bonded network with increasing X_w. As a result, we find that the heteromolecular (water–Dx) hydrogen bond dominates in the water diluted region in water–Dx mixtures, and with the progressive addition of water, bulk-like intermolecular three-dimensional hydrogen bonded water network dynamics evolves beyond $X_w = 0.1$. Additional dielectric relaxation studies indicate changes in the hydrogen bond relaxation dynamics. A fit of a double Debye relaxation model to the results of THz-TD spectra revealed the lack of cooperative water network dynamics for low water concentrations with a rapid onset of collective network motions beyond $X_w \geq 0.1$: the relaxation time τ_1 is found to be small at $X_w < 0.1$ and increases rapidly for $X_w \geq 0.1$ and then approaches that of bulk water. Weakly hydrogen bonded water molecules are expected to show a fast Debye relaxation process (small τ_1 values at low X_w), as the cooperative hydrogen bonded network is formed, i.e., for high X_w, τ_1 is found to increase. At the same time, ε_s is increased, which is attributed to water cluster formation. In the present study, FTIR measurements at low water concentrations ($X_w < 0.1$) indicated a negligible bulk water contribution in the mixture (Figures 2 and 3). This correlates with a low polarity (low ε_s values; Table 1).

In the water diluted region, the rate constant of the solvolysis of BzCl is observed to be very slow, and it increases rapidly at $X_w \geq 0.1$, indicating a change in the reaction pathway as the

14467

dx.doi.org/10.1021/jp204927r |*J. Phys. Chem. A* 2011, 115, 14462–14469

nucleophilic character of water changes in the mixtures. These experimentally observed rapid changes in the water network (dynamics) correlate directly with the experimentally observed significant increase of the reaction rate of the BzCl solvolysis reaction in water—Dx mixtures at $X_w \geq 0.1$. As evidenced from earlier DLS measurements,[26] the size of the water clusters in Dx increases with increasing X_w due to the formation of a collective hydrogen bonded network of water (as evidenced from the present FTIR studies), which explains the observed increase in the polarity of clustered water (increase in ε_s with X_w; Table 1).

Solvolysis of BzCl is an essentially nucleophilic solvent assisted reaction[54] in which the C—Cl bond breakage and formation of acylium cation serves as the rate determining step (RDS) (S_N1 mechanism), or depending upon the environment, the nucleophilic attack of water can also act as the RDS (S_N2 mechanism). In a confined and/or microheterogeneous environment an intermediate mechanism takes place, and either of the two proposed mechanisms or both may play key roles depending upon the environmental condition.[57] A discrete differentiation between the various mechanisms of such substitution reaction is difficult to establish due to the gradual nature of the transition between S_N1 and S_N2 mechanisms as the ionic character of the transition state changes.[58]

The lower polarity due to cluster formation destabilizes both the nucleofuge (Cl^-) and the intermediately formed acylium cation, thereby disabling an S_N1 pathway to follow. A similar argument has previously been put forward for the BzCl solvolysis reaction in AOT reverse micellar (RM) systems in which at low water content the rate of reaction has been found to be low, and S_N1 mechanism was disfavored. However, an increased nucleophilicity of water inside small AOT RM droplets, resulting from an increased bonding between the hydrogen atoms of interfacial water molecules and AOT head groups,[59] resulted in an increase in the reaction rate. For increasing water content, the S_N1 reaction pathway is followed as it stabilizes the acylium cation intermediate as well as the leaving group (Cl^-). This, in turn, increases the reaction rate rapidly as had also been observed in AOT RM with increasing water content beyond $w_0 > 20$ (w_0 is the water/surfactant mole ratio).[57] In general, the observed reaction rate is a balance between these two opposite effects. Thus, any change in the structure and dynamics of the water network can induce an increase in the reaction rate. We state that, any stabilizing effect such as those caused by the formation of more rigid water—water hydrogen bonds and/or those by the change in polarity of the water clusters due to cluster formation (increase of ε_s) will lead to an increased solvolyis reaction rate.

In summary, our study shows a direct correlation between the change in the structure and dynamics of water with increasing water concentration and the reaction rate. The investigation of the water—1,4-dioxane system serves as a model system, which shows the influence of hydration on the activity, demonstrating the importance of the solvent for chemical reactivity.

ASSOCIATED CONTENT

S **Supporting Information.** FTIR spectra of 1,4-dioxane in the FIR and MIR regions and deconvoluted spectrum of pure water in the MIR region. This material is available free of charge via the Internet at http://pubs.acs.org.

AUTHOR INFORMATION

Corresponding Author
*Tel: +49-234-32-24249. Fax: +49-234-32-14183. E-mail: martina.havenith@rub.de.

REFERENCES

(1) Ball, P. *Chem. Rev.* **2008**, *108*, 74.
(2) Pal, S. K.; Zewail, A. H. *Chem. Rev.* **2004**, *104*, 2099.
(3) Halle, B. *Phil. Trans. R. Soc., B* **2004**, *359*, 1207.
(4) Roberts, S. T.; Ramasesha, K.; Tokmakoff, A. *Acc. Chem. Res.* **2009**, *42*, 1239.
(5) Vaitheeswaran, S.; Yin, H.; Rasaiah, J. C.; Hummer, G. *Proc. Natl. Acad. Sci. U.S.A.* **2004**, *101*, 17002.
(6) Liu, K.; Cruzan, J. D.; Saykally, R. J. *Science* **1996**, *271*, 929.
(7) Gruenloh, C. J.; Carney, J. R.; Arrington, C. A.; Zwier, T. S.; Fredericks, S. Y.; Jordan, K. D. *Science* **1997**, *276*, 1678.
(8) Nauta, K.; Miller, R. E. *Science* **2000**, *287*, 293.
(9) Price, W. S.; Ide, H.; Arata, Y. *J. Chem. Phys.* **2000**, *113*, 3686.
(10) Nibbering, E. T. J.; Elsaesser, T. *Chem. Rev.* **2004**, *104*, 1887.
(11) Starr, F. W.; Nielsen, J. K.; Stanley, H. E. *Phys. Rev. Lett.* **1999**, *82*, 2294.
(12) Fukasawa, T.; Sato, T.; Watanabe, J.; Hama, Y.; Kunz, W.; Buchner, R. *Phys. Rev. Lett.* **2005**, *95*, 197802.
(13) Nakayama, H.; Shinoda, K. *J. Chem. Thermodyn.* **1971**, *3*, 401.
(14) Graener, H.; Seifert, G.; Laubereau, A. *Chem. Phys.* **1993**, *175*, 193.
(15) Graener, H.; Seifert, G. *J. Chem. Phys.* **1993**, *98*, 36.
(16) Cringus, D.; Yeremenko, S.; Pshenichnikov, M. S.; Wiersma, D. A. *J. Phys. Chem. B* **2004**, *108*, 10376.
(17) Cringus, D.; Bakulin, A.; Lindner, J.; Vöhringer, P.; Pshenichnikov, M. S.; Wiersma, D. A. *J. Phys. Chem. B* **2007**, *111*, 14193.
(18) Sakurai, M. *J. Chem. Eng. Data* **1992**, *37*, 492.
(19) Goates, J. R.; Sullivan, R. J. *J. Phys. Chem.* **1958**, *62*, 188.
(20) Sirotkin, V. A.; Solomonov, B. N.; Faizullin, D. A.; Fedotov, V. D. *J. Struct. Chem.* **2000**, *41*, 997.
(21) Choppin, G. R.; Violante, M. R. *J. Chem. Phys.* **1972**, *56*, 5890.
(22) Mizuno, K.; Imafuji, S.; Fujiwara, T.; Ohta, T.; Tamiya, Y. *J. Phys. Chem. B* **2003**, *107*, 3972.
(23) Takamuku, T.; Yamaguchi, A.; Tabata, M.; Nishi, N.; Yoshida, K.; Wakita, H.; Yamaguchi, T. *J. Mol. Liq.* **1999**, *83*, 163.
(24) Takamuku, T.; Nakamizo, A.; Tabata, M.; Yoshida, K.; Yamaguchi, T.; Otomo, T. *J. Mol. Liq.* **2003**, *103*, 143.
(25) Sudo, S.; Oshiki, N.; Shinyashiki, N.; Yagihara, S.; Kumbharkhane, A. C.; Mehrotra, S. C. *J. Phys. Chem. A* **2007**, *111*, 2993.
(26) Mitra, R. K.; Verma, P. K.; Pal, S. K. *J. Phys. Chem. B* **2009**, *113*, 4744.
(27) Molotsky, T.; Huppert, D. *J. Phys. Chem. A* **2003**, *107*, 8449.
(28) Mukherjee, S.; Sahu, K.; Roy, D.; Mondal, S. K.; Bhattacharyya, K. *Chem. Phys. Lett.* **2004**, *384*, 128.
(29) Garg, S. K.; Smyth, C. P. *J. Chem. Phys.* **1965**, *43*, 2959.
(30) Schrödle, S.; Hefter, G.; Buchner, R. *J. Phys. Chem. B* **2007**, *111*, 5946.
(31) Schrödle, S.; Fischer, B.; Helm, H.; Buchner, R. *J. Phys. Chem. A* **2007**, *111*, 2043.
(32) Mashimo, S.; Miura, N.; Umehara, T.; Yagihara, S.; Higasi, K. *J. Chem. Phys.* **1992**, *96*, 6358.

(33) Raichlin, Y.; Millo, A.; Katzir, A. *Phys. Rev. Lett.* **2004**, *93*, 185703.

(34) Maréchal, Y. *J. Mol. Struct.* **1994**, *322*, 105.

(35) Smith, J. D.; Saykally, R. J.; Geissler, P. L. *J. Am. Chem. Soc.* **2007**, *129*, 13847.

(36) Coker, D. F.; Miller, R. E.; Watts, R. O. *J. Chem. Phys.* **1985**, *82*, 3554.

(37) Conrad, M. P.; Strauss, H. L. *J. Phys. Chem.* **1987**, *91*, 1668.

(38) Bertie, J. E.; Lan, Z. *Appl. Spectrosc.* **1996**, *50*, 1047.

(39) Heyden, M.; Havenith, M. *Methods* **2010**, *52*, 74.

(40) Zelsmann, H. R. *J. Mol. Struct.* **1995**, *350*, 95.

(41) Ohmine, I.; Saito, S. *Acc. Chem. Res.* **1999**, *32*, 741.

(42) Walrafen, G. E. *J. Phys. Chem.* **1990**, *94*, 2237.

(43) Heyden, M.; Sun, J.; Funkner, S.; Mathias, G.; Forbert, H.; Havenith, M.; Marx, D. *Proc. Natl. Acad. Sci. U.S.A.* **2010**, *107*, 12068.

(44) Kindt, J. T.; Schmuttenmaer, C. A. *J. Phys. Chem.* **1996**, *100*, 10373.

(45) Yagasaki, T.; Ono, J.; Saito, S. *J. Chem. Phys.* **2009**, *131*, 164511.

(46) Gaiduk, V. I.; Vij, J. K. *Phys. Chem. Chem. Phys.* **2001**, *3*, 5173.

(47) Venables, D. S.; Schmuttenmaer, C. A. *J. Chem. Phys.* **2000**, *113*, 11222.

(48) Cinacchi, G.; Ingrosso, F.; Tani, A. *J. Phys. Chem. B* **2006**, *110*, 13633.

(49) Nagy, P. I.; Völgyi, G.; Takács-Novák, K. *J. Phys. Chem. B* **2008**, *112*, 2085.

(50) Ferrario, M.; Haughney, M.; McDonald, I. R.; Klein, M. L. *J. Chem. Phys.* **1990**, *93*, 5156.

(51) Cringus, D.; Jansen, T. I. C.; Pshenichnikov, M. S.; Wiersma, D. A. *J. Chem. Phys.* **2007**, *127*, 084507.

(52) Scatena, L. F.; Brown, M. G.; Richmond, G. L. *Science* **2001**, *292*, 908.

(53) Bentley, T. W.; Koo, I. S.; Norman, S. J. *J. Org. Chem.* **1991**, *56*, 1604.

(54) Bentley, T. W.; Carter, G. E.; Harris, H. C. *J. Chem. Soc., Chem. Commun.* **1984**, 387.

(55) Song, B. D.; Jencks, W. P. *J. Am. Chem. Soc.* **1989**, *111*, 8470.

(56) Bentley, T. W.; Harris, H. C. *J. Chem. Soc., Perkin Trans. 2* **1986**, 619.

(57) García-Río, L.; Leis, J. R.; Iglesias, E. *J. Phys. Chem.* **1995**, *99*, 12318.

(58) Jencks, W. P. *Chem. Soc. Rev.* **1981**, *10*, 345.

(59) Ruasse, M.-F.; Blagoeva, I. B.; Krys, S.; Sebastian-Gambaro, M.-A. *J. Chem. Soc., Perkin Trans. 2* **1993**, 1283.

(60) Venables, D. S.; Schmuttenmaer, C. A. *J. Chem. Phys.* **1998**, *108*, 4935.

(61) Barthel, J.; Bachhuber, K.; Buchner, R.; Hetzenauer, H. *Chem. Phys. Lett.* **1990**, *165*, 369.

(62) Koeberg, M.; Wu, C.-C.; Kim, D.; Bonn, M. *Chem. Phys. Lett.* **2007**, *439*, 60.

(63) Buchner, R.; Barthel, J.; Stauber, J. *Chem. Phys. Lett.* **1999**, *306*, 57.

(64) Yamaguchi, T.; Matsuoka, T.; Koda, S. *J. Chem. Phys.* **2004**, *120*, 7590.

(65) Born, B.; Weingärtner, H.; Bründermann, E.; Havenith, M. *J. Am. Chem. Soc.* **2009**, *131*, 3752.

14469

dx.doi.org/10.1021/jp204927r |*J. Phys. Chem. A* 2011, 115, 14462–14469